

Deuteron-Nucleus Collisions in a Multi-Phase Transport Model

Zi-wei Lin

Physics Department, The Ohio State University, Columbus, Ohio 43210

Che Ming Ko

Cyclotron Institute and Physics Department, Texas A&M University, College Station, Texas 77843

(Dated: April 6, 2019)

Using a multi-phase transport (AMPT) model, we study global observables in deuteron-gold collisions at RHIC. In particular, we present predictions on the centrality dependence of the pseudo-rapidity distributions of charged particles and the transverse energy, and discuss the effects due to centrality selection and possible modifications of the string fragmentation function.

PACS numbers: 25.75.-q, 24.10.Lx

I. INTRODUCTION

To study heavy ion collisions at the Relativistic Heavy Ion Collider (RHIC) at Brookhaven National Laboratory, in which a deconfined plasma of quarks and gluons is expected to be formed, we have developed a multi-phase transport (AMPT) model that includes both initial partonic and final hadronic interactions [1, 2]. The model has been very useful for understanding various observables in Au+Au collisions at RHIC such as the rapidity and transverse momentum distributions of various particles [1, 2] as well as charmonium [3] and strangeness [4] productions. In particular, it allows one to study both thermal and chemical equilibration in the partonic and hadronic matter formed in these collisions. The AMPT model has also been extended to include the string melting mechanism [5, 6], in which soft strings produced from initial nucleon-nucleon interactions are converted directly to partons, in order to explain the measured elliptic flow [7] and two-pion correlation functions [8].

In spite of its success, the AMPT model has many uncertainties in its input physical parameters, particularly those related to the initial conditions introduced to the model. For example, the number of initial minijet partons in the AMPT model, that is given by the hard processes from the HIJING model [9, 10, 11], depends on the nuclear shadowing, i.e., the modification of the parton distributions in a nucleon when it is in a nucleus. As a result, the final particle multiplicity produced in relativistic heavy ion collisions is affected by the nuclear shadowing [2]. The production of high p_T particles or hadrons made of heavy quarks, which is described by perturbative QCD processes, is even more sensitive to the nuclear shadowing effect. Furthermore, other nuclear effects such as the Cronin effect [12], which set in already in p-A collisions, need to be better understood. The uncertainties in the initial condition also exist in other transport models with partonic degrees of freedom [13, 14] as well as theoretical models such as the hydrodynamical model [15, 16, 17, 18] and the QCD saturation model [19, 20, 21, 22, 23].

Because of the less importance of final-state interac-

tions in deuteron-gold collisions than in heavy ion collisions, uncertainties due to both the Cronin effect and the nuclear shadowing effect (e.g., through dilepton measurements [24]) can be better studied in these collisions. Improved knowledge on these effects are useful for making reliable theoretical interpretations of the observations in heavy ion collisions at RHIC. In this paper, we use the AMPT model to study the global observables in deuteron-gold collisions, such as the centrality dependence of the pseudo-rapidity distributions of charged particles and the transverse energy. Since the interaction volume of $d+Au$ collision is small, and the effect of string melting on multiplicity distributions of charged particles is also small, the default AMPT model without the string melting mechanism is used in the present study.

This paper is organized as follows. In Section II, we briefly review the AMPT model but discuss in some detail the parameters in the string fragmentation function. Results from the AMPT model on deuteron-gold collisions at RHIC are then shown in Section III, including the charged particle pseudo-rapidity distribution and its dependence on centrality, the effect of centrality selection on the centrality dependence, and the effects due to nuclear shadowing and modifications of the parameters in the string fragmentation function. Finally, a summary is given in Section IV.

II. THE AMPT MODEL

The AMPT model is a hybrid model that consists of four components: the initial conditions, the parton cascade, the conversion from partonic to hadronic matter, and the hadron cascade. In the default AMPT model [1, 2, 3, 4], the initial conditions are generated from the HIJING model [9, 10, 11], which uses a Woods-Saxon radial shape for the colliding nuclei and introduces a parametrized nuclear shadowing function that depends on the impact parameter of the collision [9]. Interactions among the minijet partons, which are produced from the initial hard nucleon-nucleon interactions, are modeled by the Zhang's parton cascade (ZPC) [13]. After partons stop interacting, they recombine with their par-

ent strings, which are produced from initial soft nucleon-nucleon interactions, and fragment to hadrons according to the Lund string fragmentation model [25, 26]. Dynamics of the resulting hadronic matter is then described by a hadronic cascade based on the relativistic transport (ART) model [27]. Final hadronic observables including contributions from the strong decay of resonances are determined when the hadronic matter freezes out.

In the default AMPT model, hadron production after the partonic phase is described by the Lund string fragmentation model. In this model, the longitudinal momentum distribution of a hadron with transverse mass m_{\perp} produced from the string fragmentation is given by the following symmetric splitting function [26]:

$$f(z) \propto z^{-1}(1-z)^a \exp(-b m_{\perp}^2/z), \quad (1)$$

where z denotes the light-cone momentum fraction of the produced hadron with respect to that of the fragmenting string. In the HIJING model, which reproduces the experimental charged particle multiplicities in high energy pp and $p\bar{p}$ collisions, the default values of $a = 0.5$ and $b = 0.9 \text{ GeV}^{-2}$ are used. However, in order to reproduce the multiplicity distributions of charged particles in central Pb+Pb collisions at the CERN-SPS energy using the AMPT model, we find that values of these parameters need to change to $a = 2.2$ and $b = 0.5 \text{ GeV}^{-2}$ [2]. The increase of a and decrease of b relative to the default values in the HIJING model soften the splitting function and thus enhance the total charged particle multiplicity by about 20% in central Pb+Pb collisions at SPS. The change of these two parameters can perhaps be attributed to the modification of string fragmentation when multiple strings are produced and overlap in heavy ion collisions, although it is not known yet how these parameters should be modified in different colliding systems. Since peripheral $d + Au$ collisions are expected to behave similarly as pp collisions, and even in central $d + Au$ collisions the string density is much lower than in central heavy ion collisions, we first assume that the parameters a and b of Eq. (1) for deuteron-gold collisions have the same values as in pp collisions, i.e., they take the default values in the HIJING model. However, modifications of their values are possible in non-peripheral $d + Au$ collisions, and the effect is discussed in Section III D.

III. AMPT RESULTS ON DEUTERON-GOLD COLLISIONS

We have studied deuteron-gold collisions at $\sqrt{s_{NN}} = 200 \text{ GeV}$ with both deuteron and gold having the same energy of 100 GeV per nucleon. We define the ‘‘minimum-bias’’ $d + Au$ events as those within the impact parameter range between 0 and 12 fm, and then separate these events into different centrality bins.

A. Pseudo-rapidity distributions of charged particles

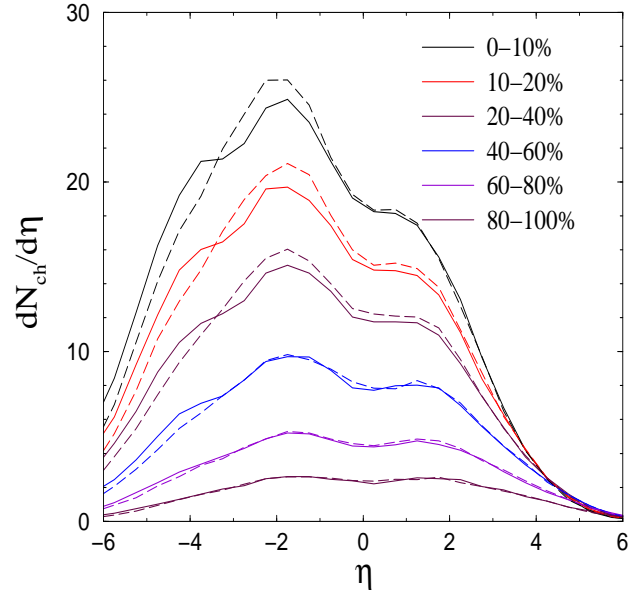


FIG. 1: Pseudo-rapidity distributions of charged particles in $d + Au$ collisions at $\sqrt{s_{NN}} = 200 \text{ GeV}$ with centralities determined from N_{part} .

Fig. 1 shows the pseudo-rapidity distributions of charged particles in the six centrality bins of 0-10%, 10-20%, 20-40%, 40-60%, 60-80% and 80-100%. Here the centrality is determined according to the value of N_{part} , i.e., the total number of participants in both deuteron and gold nuclei, in each event. The pseudo-rapidity in this study is evaluated in the nucleon-nucleon center-of-mass frame, and negative rapidities correspond to the fragmentation region of the gold nucleus. Solid curves are results from the AMPT model, while dashed curves are the AMPT results with final-state interactions (i.e., both the parton and hadron cascades) turned off. It is seen that the asymmetry in the pseudo-rapidity distributions, e.g., by comparing values of $dN_{ch}/d\eta$ at $\eta = -2$ and $\eta = +2$, decreases as collisions become less central, and the pseudo-rapidity distribution for the most peripheral bin is symmetric within 15%. As expected, final-state interactions in $d + Au$ collisions have a smaller effect on charged particle multiplicity distributions than in the case of central heavy ion collisions at RHIC [2].

We note that the appearance of the small bumps around $\eta \sim -4$ is mainly due to the interactions of produced particles with the initial incoming nucleons in the gold nucleus, as we have used an initial half width of R_{Au}/γ in the longitudinal direction for the production points of particles, where R_{Au} is the hard-sphere radius of the gold nucleus and γ represents the Lorentz boost factor of a nucleon in the nucleon-nucleon center-of-mass frame. When an initial half width a factor of 5 smaller is

used, the charged particle pseudo-rapidity distributions are smooth around $\eta \sim -4$ but otherwise have the same magnitude and shape.

B. N_{part} dependence of global observables

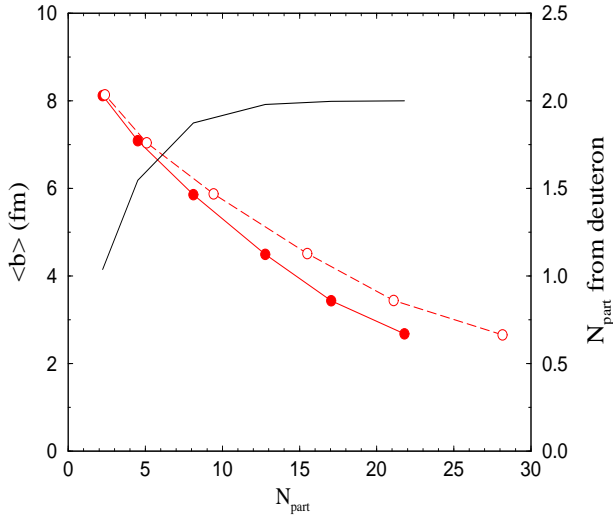


FIG. 2: The average value of impact parameter (in fm) and the number of participants from deuteron (solid curve) as a function of N_{part} . See text for details.

In Fig. 2, we show by the solid curve with circles the average impact parameter as a function of the average value of N_{part} at each centrality bin. Here, the number of participants is defined as the number of initial (projectile and target) nucleons involved in *primary* collisions, i.e., not including those initial nucleons that interact with produced particles in the final state. The solid curve with no symbols in Fig. 2 represents the contributions to N_{part} from the deuteron. We see that N_{part} from the deuteron increases toward the value of 2 rather quickly from peripheral to central collisions. The dashed curve with open circles shows the number of participating nucleons if it includes initial nucleons involved in final-state interactions in addition to those involved in primary collisions. It is seen that final-state interactions increase the number of participating nucleons by almost 30% for the most central events (0-10% centrality bin). However, since the energies involved in final-state interactions are much lower than those in the primary collisions, they contribute much less to particle production. In this study, we thus only include initial nucleons that are involved in primary collisions in the evaluation of N_{part} .

The centrality dependence of some global observables at mid-pseudo-rapidity ($-0.5 < \eta < 0.5$) are shown Fig. 3. Solid and dashed curves represent, respectively, $dN_{\text{ch}}/d\eta$ and $dE_{\text{T}}/d\eta$ with both being divided by N_{part} , where $dE_{\text{T}}/d\eta$ includes the contribution from neutral particles. In this study, $E_{\text{T}} = E \sin \theta$ with θ being the polar an-

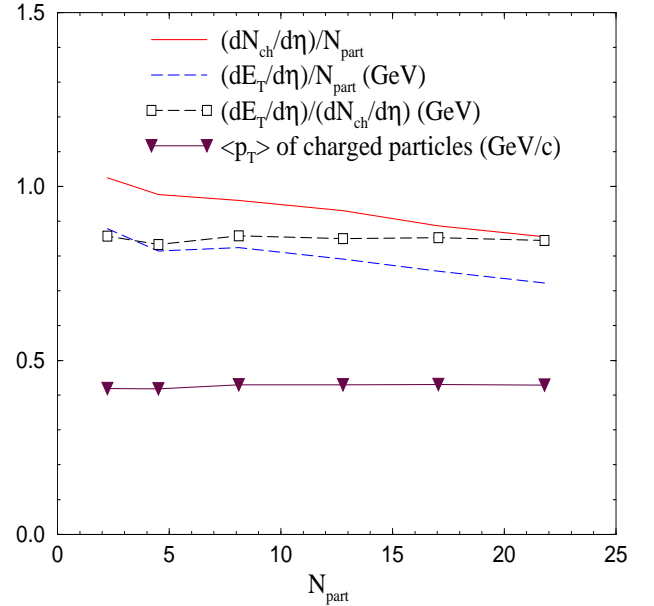


FIG. 3: Centrality dependences of charged particle multiplicity and transverse energy (in GeV) per participant, the mean transverse energy (in GeV) per charged particle, and the mean p_{T} (in GeV/c) of charged particles at mid-pseudo-rapidity.

gle, and E is defined as the kinetic energy for baryons, the total energy plus the nucleon mass for anti-baryons, and the total energy for all other particles. We observe that both the multiplicity and transverse energy per participant gradually decrease with N_{part} . However, we shall see in Sections III C and III D that this moderate decrease with centrality may change when centralities are selected differently or when the string fragmentation function is modified in more central $d + Au$ collisions. Fig. 3 also shows that their rates of change are similar as seen from their ratio, i.e., the average transverse energy per charged particle, shown by the rather flat dashed curve with squares. As shown by the curve with triangles, the mean transverse momentum of charged particles also changes little with N_{part} .

The centrality dependence of the charged particle multiplicity per participant at different pseudo-rapidities is shown in Fig. 4, where the value at each η represents the average value within the pseudo-rapidity range of $\eta \pm 0.5$. We see an increase of this quantity at the backward pseudo-rapidity $\eta = -4$ (curve with open diamonds) and a fast decrease at the forward pseudo-rapidity $\eta = +4$ (curve with filled diamonds). Furthermore, the decrease with centrality becomes stronger as the pseudo-rapidity changes from negative values to more positive values. These are consistent with the picture that multiple interactions in the gold nucleus push particle productions toward the negative rapidity region. As we find that the mean transverse energy per charged particle at a given pseudo-rapidity does not change much with centrality, the centrality dependence of $(dE_{\text{T}}/d\eta)/N_{\text{part}}$ (i.e., the transverse energy per par-

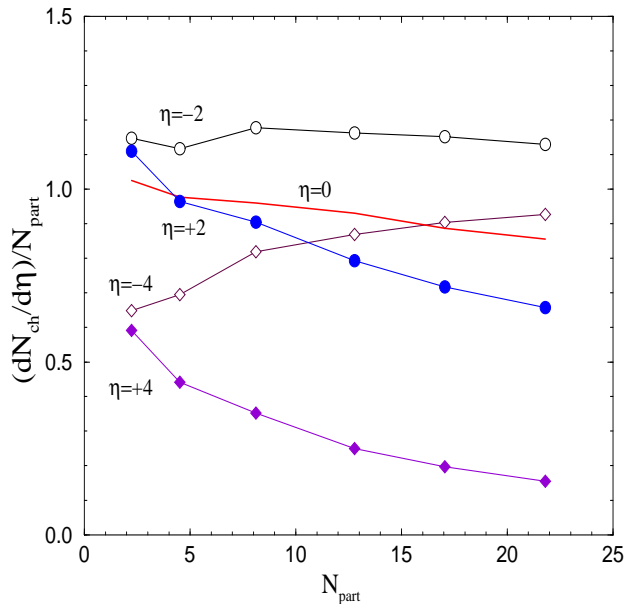


FIG. 4: Centrality dependence of charged particle multiplicity per participant at different pseudo-rapidities.

participant, shown in Fig. 5) has similar behavior at each pseudo-rapidity as $(dN_{ch}/d\eta)/N_{part}$.

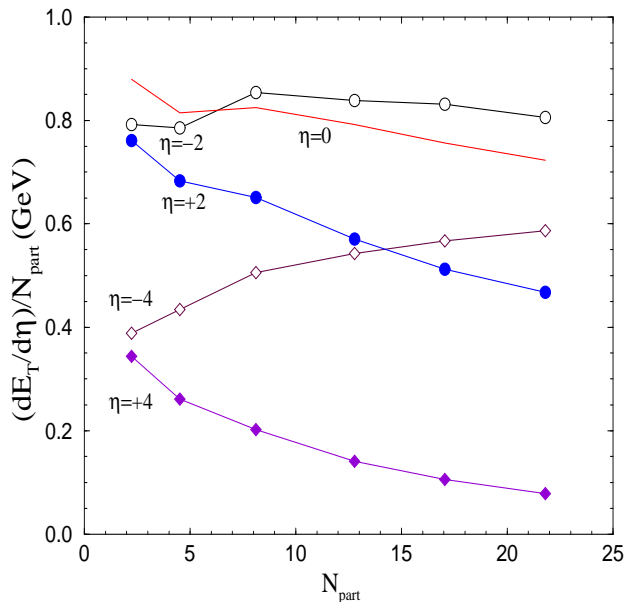


FIG. 5: Centrality dependence of the transverse energy (in GeV) per participant at different pseudo-rapidities.

C. Effect of centrality selection

To extract useful information from the centrality dependence of global observables, it is helpful to study how the criteria of centrality selection affects the centrality

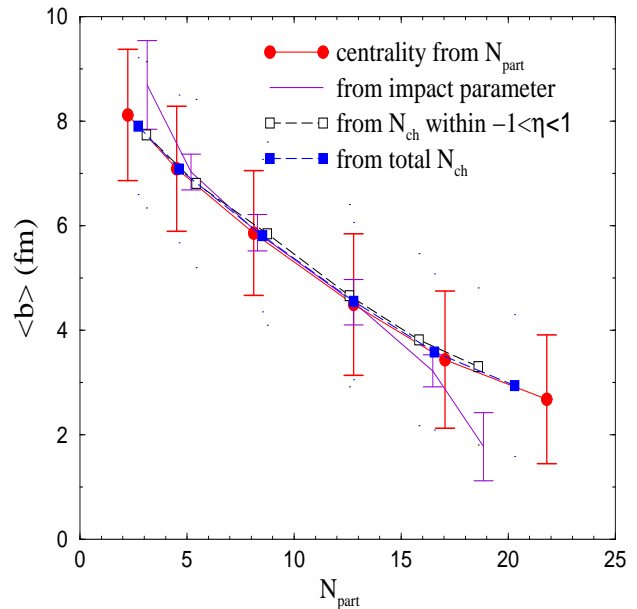


FIG. 6: The average value of impact parameter as a function of N_{part} with different criteria for the centrality selection, together with the RMS width of the impact parameter in each centrality bin for two of the curves.

dependence. The number of participants and the impact parameter are known in theoretical models, but they can not be measured directly experimentally. Instead, experimental centrality selections usually involve cutting on the charged particle multiplicity or the transverse energy. Thus, in addition to separating events into different centrality bins using the total number of participants, we have also tried three other methods, using the impact parameter, the number of charged particles within $-1 < \eta < 1$, and the total number of charged particles. For example, when the total number of charged particles is used for the centrality selection, we order all 10,000 events from our model by the total number of charged particles in each event. The centrality bin of, say 0-10%, then consists of the first 1,000 events in that ordered list.

In Fig. 6, we plot the average value of impact parameters versus the average value of N_{part} at six centrality bins of 0-10-20-40-60-80-100%, that are selected using these four different methods. The solid curve with circles corresponds to the centrality selection from N_{part} , and it thus has the largest value of N_{part} for the most central bin of events and the smallest value of N_{part} for the most peripheral bin of events. On the other hand, the centrality selection from the impact parameter, shown by the solid curve with no symbols, has the smallest value of $\langle b \rangle$ for the most central bin of events and the largest value of $\langle b \rangle$ for the most peripheral bin of events. When the number of charged particles is used to determine the centrality, the correlation between the centrality and N_{part} is weaker than in the case of using N_{part} . This is especially true when only part of the phase space is included, as using N_{ch} within $-1 < \eta < 1$ for the centrality selection (curve

with open squares) leads to a narrower range of N_{part} than using the total number of charged particles for the centrality selection (curve with filled squares). The error bars shown for two of the curves in Fig. 6 (the curves from using N_{part} or impact parameter for the centrality selection) correspond to the root-mean-square widths of the impact parameters in each centrality bin, and we see that the width in the case of using N_{part} for determining the centrality is quite large (around 1.2 fm) for these centrality bins. We also find that, when N_{ch} within $-1 < \eta < 1$ or the total N_{ch} is used for the centrality selection, these widths are even larger (between 1.3 and 1.8 fm), indicating that the correlation between N_{ch} and the impact parameter is weaker than that between N_{part} and the impact parameter.

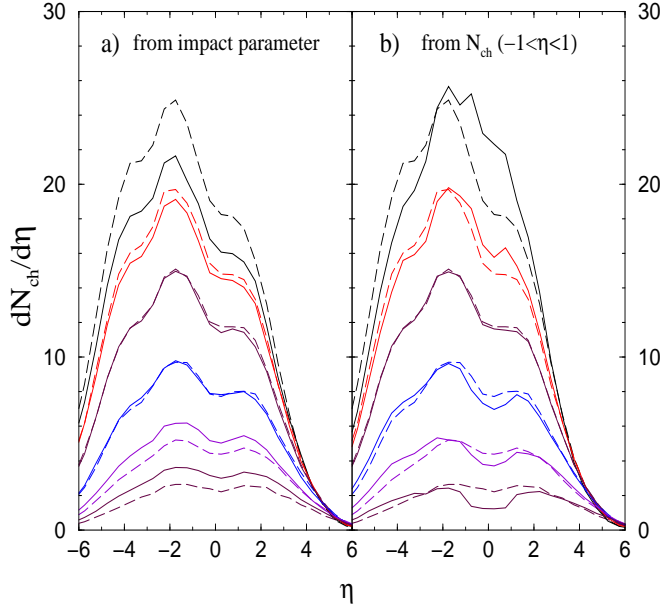


FIG. 7: Charged particle multiplicity distributions at six centrality bins of 0 – 10 – 20 – 40 – 60 – 80 – 100% when the centrality is determined from a) the impact parameter or b) N_{ch} within $-1 < \eta < 1$. Dashed curves represent results when the centrality is determined from N_{part} .

Different centrality selections also lead to differences in both the shape and the magnitude of the pseudo-rapidity distributions at the same centrality bin. Solid curves in Fig. 7a and 7b show the pseudo-rapidity distributions of charged particles using, respectively, the impact parameter and N_{ch} within $-1 < \eta < 1$ for determining the centrality. The distributions corresponding to using N_{part} for the centrality selection are also shown by the dashed curves for comparison. From Fig. 7a, we find that $dN_{ch}/d\eta$ at $\eta = 0$ grows slower with centrality when the impact parameter instead of N_{part} is used for the centrality selection. However, it is interesting to see, from comparing Fig. 8a with Fig. 4, that the centrality dependences of $(dN_{ch}/d\eta)/N_{\text{part}}$ for the two cases are quite similar. This is due to the compensating effect of the slower growth of N_{part} with centrality when the impact

parameter is used to select the centrality (see Fig. 6). We note that, in relativistic heavy ion collisions where the multiplicity is much higher, these different methods for the centrality selection lead to quite similar results, contrary to those shown in Figs. 6 and 7 for $d + Au$ collisions.

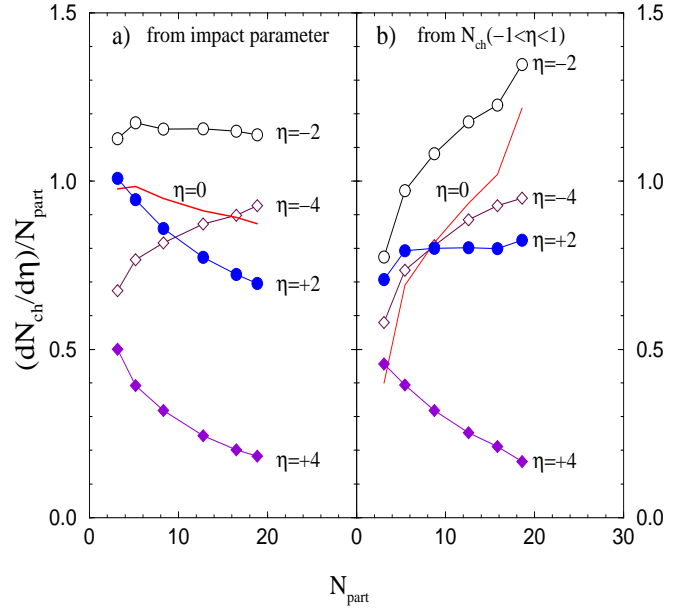


FIG. 8: Centrality dependence of charged particle multiplicity with the centrality determined from a) the impact parameter or b) N_{ch} within $-1 < \eta < 1$.

Fig. 8b shows the centrality dependence of charged particle multiplicity per participant at different pseudo-rapidities when N_{ch} within $-1 < \eta < 1$ is used for the centrality selection. Comparing with Fig. 4, we find that the centrality dependence at $\eta = -4$ or $\eta = +4$ is similar to the case where N_{part} determines the centrality, but the centrality dependence at $\eta = -2, 0$ or $+2$ is totally different. For example, while in Fig. 4 (and in Fig. 8a) the curve of $(dN_{ch}/d\eta)/N_{\text{part}}$ at $\eta = 0$ shows a small decrease with centrality, the corresponding curve in Fig. 8b increases significantly with centrality. We note that these differences from Fig. 4 exist even when the total number of N_{ch} is used for selecting the centrality (instead of N_{ch} within $-1 < \eta < 1$). Part of this large difference in the centrality dependence is due to the stronger increase of $dN_{ch}/d\eta(\eta = 0)$ with centrality in the case when N_{ch} around mid-pseudo-rapidity is used to determine the centrality, as shown in Fig. 7b. Also, since the average value of N_{part} grows slower with centrality in this case (see Fig. 6), the difference is further enhanced after dividing $dN_{ch}/d\eta$ by N_{part} . Figs. 7 and 8 thus show that the criteria of centrality selection can introduce appreciable differences in the centrality dependence of global observables in deuteron-gold collisions, and corresponding care must be taken when comparing theoretical results with experimental data.

D. Effects of the string fragmentation parameters and nuclear shadowing

In obtaining the above results, we have assumed that the parameters a and b in Eq.(1) for the string fragmentation have same values as in pp collisions. Since their values need to be modified in order to describe the total multiplicity in central heavy ion collisions, it is thus possible that these parameters are also modified in non-peripheral deuteron-gold collisions. If in central deuteron-gold collisions the parameters a and b already have the modified values as in heavy ion collisions, the multiplicity distribution for the 10% most central deuteron-gold collisions (selected from N_{part}) would be given by the dashed curve in Fig. 9, which shows a substantial increase compared with the previous AMPT result obtained with default a and b values in the HIJING model (solid curve). Comparison of these predictions for deuteron-gold collisions with upcoming experimental results at RHIC will thus allow us to learn how the string fragmentation process is modified in different colliding systems or centralities.

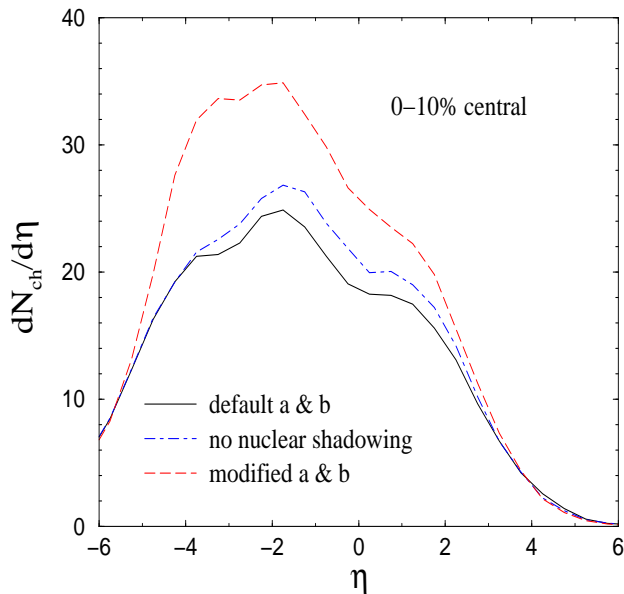


FIG. 9: Charged particles multiplicity distributions for the most central 10% deuteron-gold collisions from the AMPT model with default values of a and b parameters (solid), with nuclear shadowing turned off (dot-dashed), or with modified a and b values as in heavy ion collisions (dashed).

When the nuclear shadowing effect is turned off in the AMPT model, the multiplicity distribution for the 10% most central deuteron-gold collisions is shown by the dot-dashed curve in Fig. 9, which is not much different from the solid curve obtained with the nuclear shadowing. Thus, multiplicity distributions of charged parti-

cles in deuteron-gold collisions are not very sensitive to the nuclear shadowing effect. This is different from that seen in collisions between heavy nuclei, where the effect is much larger as nuclear shadowing affects the production of minijet partons, which scales with the number of binary collisions. Although the nuclear shadowing effect is unimportant for global observables in smaller colliding systems such as deuteron-gold collisions, it affects significantly observables which are dominated by partonic interactions such as open charm production [24] or the yield of high p_T particles.

IV. SUMMARY

In summary, using a multi-phase transport (AMPT) model that includes both initial partonic and final hadronic interactions, we have studied the pseudo-rapidity distribution of charged particles and the transverse energy as well as their centrality dependence in deuteron-gold collisions at $\sqrt{s_{NN}} = 200$ GeV. Due to the asymmetry of these collisions, the centrality dependence of charged particle multiplicity per participant is very different at different pseudo-rapidities, and it goes from increasing with centrality at the backward pseudo-rapidity region (the fragmentation region of the gold nuclei) to decreasing with centrality at the forward region. Using several methods for centrality selection, we have also found that, while using the impact parameter or N_{part} to determine the centrality gives a similar centrality dependence for $(dN_{ch}/d\eta)/N_{\text{part}}$ at various pseudo-rapidities, using N_{ch} for the centrality selection leads to very different results. We further find that, although the charged particle multiplicity distribution in central deuteron-gold collisions is not sensitive to the nuclear shadowing effect, it is affected significantly by the values of the parameters used in the string fragmentation function. Comparison of these predictions with the experimental data will thus help us to learn whether the string fragmentation is modified in deuteron-gold collisions as in central heavy ion collisions. This will in turn provide useful information on the impact parameter dependence of the string fragmentation function in heavy ion collisions.

Acknowledgments

We thank Ulrich Heinz and Michael Murray for valuable comments. This paper is based on work supported by the U.S. Department of Energy under Grant No. DE-FG02-01ER41190 (Z.W.L.) and by the U.S. National Science Foundation under Grant No. PHY-0098805 as well as the Welch Foundation under Grant No. A-1358 (C.M.K.)

-
- [1] B. Zhang, C. M. Ko, B. A. Li and Z. W. Lin, arXiv:nucl-th/9904075; Phys. Rev. C **61**, 067901 (2000).
- [2] Z. W. Lin, S. Pal, C. M. Ko, B. A. Li and B. Zhang, Phys. Rev. C **64**, 011902 (2001); Nucl. Phys. A **698**, 375 (2002).
- [3] B. Zhang, C. M. Ko, B. A. Li, Z. W. Lin and B. H. Sa, Phys. Rev. C **62**, 054905 (2000); B. Zhang, C. M. Ko, B. A. Li, Z. W. Lin and S. Pal, Phys. Rev. C **65**, 054909 (2002).
- [4] S. Pal, C. M. Ko and Z. W. Lin, arXiv:nucl-th/0106073; Nucl. Phys. A **707**, 525 (2002).
- [5] Z. W. Lin and C. M. Ko, Phys. Rev. C **65**, 034904 (2002).
- [6] Z. W. Lin, C. M. Ko and S. Pal, Phys. Rev. Lett. **89**, 152301 (2002).
- [7] K. H. Ackermann *et al.* [STAR Collaboration], Phys. Rev. Lett. **86**, 402 (2001).
- [8] C. Adler *et al.* [STAR Collaboration], Phys. Rev. Lett. **87**, 082301 (2001).
- [9] X. N. Wang and M. Gyulassy, Phys. Rev. D **44**, 3501 (1991).
- [10] X. N. Wang and M. Gyulassy, Phys. Rev. D **45**, 844 (1992).
- [11] M. Gyulassy and X. N. Wang, Comput. Phys. Commun. **83**, 307 (1994).
- [12] J. W. Cronin, H. J. Frisch, M. J. Shochet, J. P. Boymond, R. Mermod, P. A. Piroué and R. L. Sumner, Phys. Rev. D **11**, 3105 (1975).
- [13] B. Zhang, Comput. Phys. Commun. **109**, 193 (1998).
- [14] D. Molnar and M. Gyulassy, Phys. Rev. C **62**, 054907 (2000).
- [15] P. F. Kolb, P. Huovinen, U. W. Heinz and H. Heiselberg,
- [16] P. Huovinen, P. F. Kolb, U. W. Heinz, P. V. Ruuskanen and S. A. Voloshin, Phys. Lett. B **503**, 58 (2001).
- [17] P. F. Kolb, U. W. Heinz, P. Huovinen, K. J. Eskola and K. Tuominen, Nucl. Phys. A **696**, 197 (2001).
- [18] D. Teaney, J. Lauret and E. V. Shuryak, arXiv:nucl-th/0110037.
- [19] D. Kharzeev and E. Levin, Phys. Lett. B **523**, 79 (2001).
- [20] D. Kharzeev and M. Nardi, Phys. Lett. B **507**, 121 (2001).
- [21] D. Kharzeev, E. Levin and M. Nardi, arXiv:hep-ph/0212316.
- [22] K. J. Eskola, K. Kajantie, P. V. Ruuskanen and K. Tuominen, Nucl. Phys. B **570**, 379 (2000); Phys. Lett. B **543**, 208 (2002).
- [23] K. J. Eskola, K. Kajantie and K. Tuominen, Phys. Lett. B **497**, 39 (2001).
- [24] Z. W. Lin and M. Gyulassy, Phys. Rev. Lett. **77**, 1222 (1996).
- [25] T. Sjostrand, Comput. Phys. Commun. **82**, 74 (1994).
- [26] B. Andersson, G. Gustafson and B. Soderberg, Z. Phys. C **20**, 317 (1983); B. Andersson, G. Gustafson, G. Ingelman and T. Sjostrand, Phys. Rept. **97**, 31 (1983).
- [27] B. A. Li and C. M. Ko, Phys. Rev. C **52**, 2037 (1995).